Communication

Seedless Growth of Palladium Nanocrystals with Tunable Structures: From Tetrahedra to Nanosheets

Ying Zhang, Mingsong Wang, Enbo Zhu, Yuebing Zheng, Yu Huang, and Xiaoqing Huang

Nano Lett., **Just Accepted Manuscript** • DOI: 10.1021/acs.nanolett.5b04019 • Publication Date (Web): 21 Oct 2015

Seedless Growth of Palladium Nanocrystals with Tunable Structures: From Tetrahedra to Nanosheets

Ying Zhang,[†] Mingsong Wang,[‡] Enbo Zhu,[§] Yuebing Zheng,[‡] Yu Huang[§] and Xiaoqing Huang[*†]*

[†]College of Chemistry, Chemical Engineering and Materials Science, Soochow University, Jiangsu, 215123, China.

[‡]Department of Mechanical Engineering, Materials Science and Engineering Program, and Texas Materials Institute, The University of Texas at Austin, Austin, Texas 78712, United States.

[§]Department of Materials Science and Engineering, University of California, Los Angeles, California 90095, United States.

[*]Address correspondence to: hxq006@suda.edu.cn; yhuang@seas.ucla.edu.

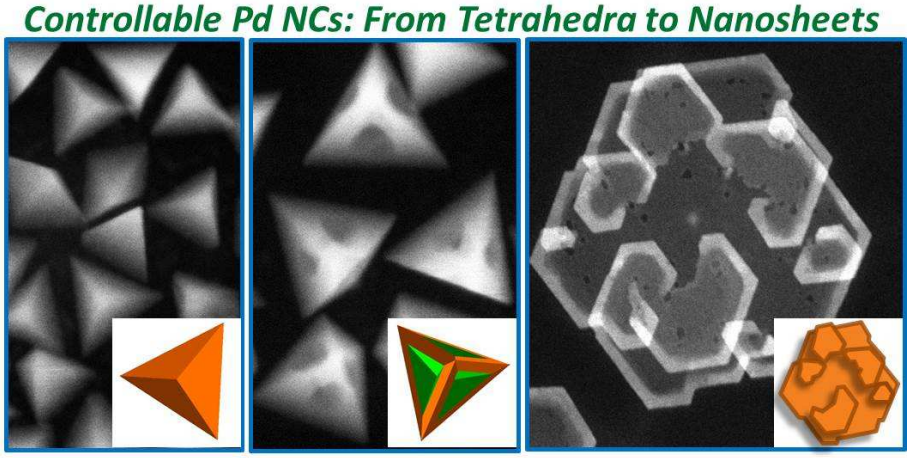

Abstract: Despite great success has been accomplished on the controlled synthesis of Pd nanocrystals with various sizes and morphologies, an efficient approach to systematic production of well-defined Pd nanocrystals without seed-mediated approaches remains a significant challenge. In this work, we have developed an efficient synthetic method to directly produce Pd nanocrystals with highly controllable

feature. Three distinct Pd nanocrystals, namely, Pd nanosheets, Pd concave tetrahedra, and Pd tetrahedra have been selectively prepared by simply introducing a small amount of ascorbic acid (AA) and/or water without the other synthesis condition changed. We found that the combined use of AA and water is of importance for the successful production of the unique Pd nanosheets. Detailed catalytic investigations showed that all the obtained Pd nanocrystals exhibit higher activity in the formic acid electrooxidation and styrene hydrogenation with respect to the Pd black, and their activities are highly shape-dependent with Pd nanosheets demonstrating a higher activity than both the Pd concave tetrahedra and Pd tetrahedra, which is likely due to the simple yet important feature of ultrathin thickness of Pd nanosheets. The present work highlights the importance of structures in tuning the related properties of metallic nanocrystals.

Keywords: Palladium, Nanosheet, Tetrahedron, Hydrogenation, Electrooxidation

The synthesis of well-defined Pd nanocrystals has continually attracted extensive research attention in multiple fields of fundamental science and technology mainly due to their promising properties and various potential applications, including highly active catalysts in various organic reactions, electrocatalysts in fuel cell reactions, and hydrogen storage/sensing.[1-10] All of these broad applications require precise control over Pd nanocrystals to enhance their properties.[11] In general, the properties of Pd nanocrystals are mainly determined by two factors: 1) the intrinsic nature of active sites, which are dictated by the exposed facets of the Pd nanocrystals; 2) the accessible active sites, which are determined by specific surface area of the Pd nanocrystals.[12-15] As a consequent, many researchers pay great attention to the two aforementioned aspects when designing and preparing various Pd nanocrystals.[1-3,11]

Studying the well-defined Pd nanocrystal system is important for answering fundamental questions that could allow the preparation of Pd nanocrystals with improved performance.[11]

Towards improving the properties of Pd nanocrystals, much progress has been achieved on the control of Pd nanocrystals over the past decades.[1-3,11] Pd nanocrystals with various morphologies, including nanosphere, nanocube, octahedron, tetrahedron, nanorod/nanowire, nanosheet and so forth, have been successfully created by various strategies.[16-30] For example, the tetrahexahedral Pd nanocrystals show much high ethanol electrooxidation activity than commercial Pd black owing to the presence of highly active surface structure.[18] Because of the ultrathin nature, the Pd nanosheets exhibit a well-defined surface plasmon resonance peak in the near-infrared region and highly improved surface area.[24] Although the previous results have contributed much to the preparation of Pd nanocrystals with much improved properties, it should be pointed out that these syntheses were conducted under very different conditions, which are not suitable for the shape dependent property studies. Furthermore, it should be noted that the majority of previous reported Pd nanocrystals lack systematic structure tunability, which are however important to the rational design of high-performance Pd nanocrystals with potentially practical applications. In fact, the synthesis of the Pd nanocrystals with systematic tuned structures can be achieved through the seed-mediated strategy.[31-34] The seed mediated strategy, i.e. Pd seed syntheses and the following growth on the Pd seeds, however, are neither cost-effective nor efficient. To scale up their production, an effective method has yet to be exploited. Therefore, the development of effective wet-chemical approach for the direct preparation of Pd nanocrystals with systematic tunable structure is highly desirable, but remains a tremendous challenge.[29-30]

Herein, we demonstrate an effective wet-chemical method for the production of well-defined Pd nanocrystals in a highly controllable manner. Three distinct nanostructures, namely, unique Pd nanosheets, Pd concave tetrahedra and Pd tetrahedra have been selectively prepared. To the best of our

knowledge, this is the first time that Pd nanosheets have been prepared without the use of toxic carbon monooxide or metal carbonyls.[24,27] Furthermore, unlike many previous work on the systematic control of Pd nanocrystals that largely relied on the seed-mediated approaches, our current tunable control of Pd nanocrystals have been achieved directly under similar growth conditions except for introducing various small molecules such as AA and/or H_2O. Therefore, one can readily image that our systematic tuning of Pd nanocrystals with well-defined structures provides an ideal platform for investigating the effect of structures on their related properties and catalytic activities. We found that the obtained Pd nanocrystals exhibit highly shape-dependent catalytic activities in the formic acid electrooxidation and styrene hydrogenation with Pd nanosheets showing higher activities than those of the Pd concave tetrahedra, Pd tetrahedra and also Pd black, which is likely due to the simple yet important feature of ultrathin thickness of the Pd nanosheets.

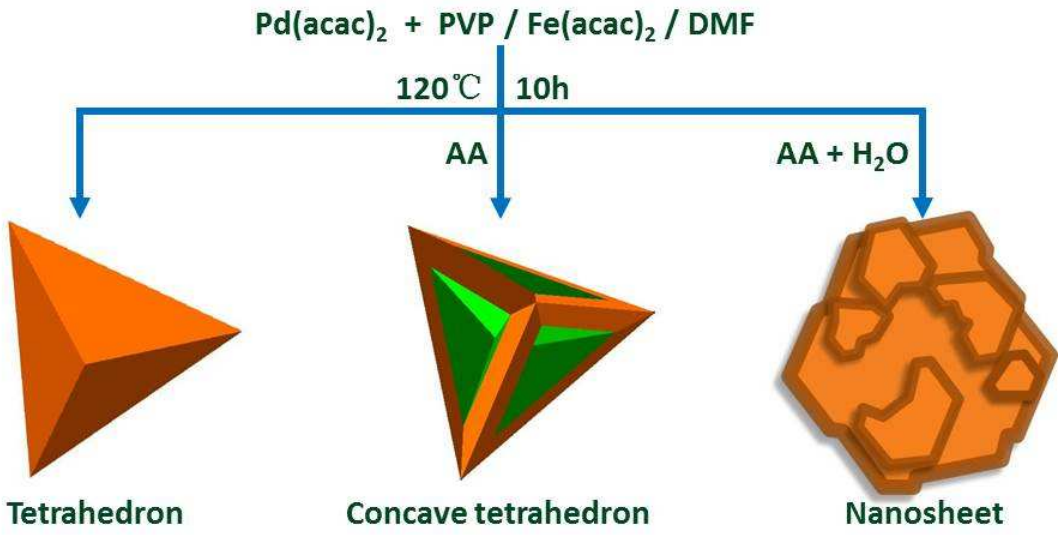

Scheme 1. Schematic illustration of the growth conditions to the synthesis of well-defined Pd nanocrystals with controlled manner.

The well-defined Pd nanocrystals were made by reduction of palladium (II) acetylacetonate ($Pd(acac)_2$) by using N, N-dimethylformamide (DMF) as both solvent and reducing agent, which

contained polyvinylpyrrolidone (PVP) as surfactant and iron(II) acetylacetonate ($Fe(acac)_2$) as shape-directing agent, in the juridical presence of AA and/or water for the selective creation of Pd nanosheets, Pd concave tetrahedra and Pd tetrahedra (**Scheme 1, Figure S1**). The typical characterizations of the obtained Pd tetrahedra are shown in **Figure 1 and Figure S2**. The representative transmission electron microscopy (TEM) (**Figure 1a**) and high-angle annular dark-field scanning TEM (HAADF-STEM) images (**Figure 1b**) show that the majority of the products have tetrahedral shape (**Figure 1c**). The tetrahedra are monodisperse, with an average edge length of 30±4 nm. The powder X-ray diffraction (PXRD) pattern of the nanocrystals shows a face-centered-cubic (*fcc*) structure with the peak positions matching well with the metallic Pd diffractions (**Figure S1**), confirming the formation of Pd nanocrystals. The lattice spacing are measured to be 0.23 nm, corresponding to the (111) plane of *fcc* Pd nanocrystals (**Figure S2**). When a small amount of AA was introduced with the other synthesis condition the same to that of Pd tetrahedra, we produced Pd concave tetrahedra of 40±5 nm in edge length. The successful synthesis of Pd nanocrystals was confirmed by the PXRD, as shown in **Figure S1**. **Figure 1d-e** are the typical TEM and HAADF-STEM images of the Pd concave tetrahedra, which clearly demonstrate the high-quality of the products with concave feature (**Figure 1f**). The lattice spacing along the edge of an octahedron shown in the HRTEM image is 0.14 nm (**Figure S2**), close to that of the (220) plane of Pd nanocrystals. As confirmed by inductively coupled plasma atomic emission spectroscopy (ICP-AES), no Fe was detected in these two Pd polyhedra despite $Fe(acac)_2$ was used in the synthesis.

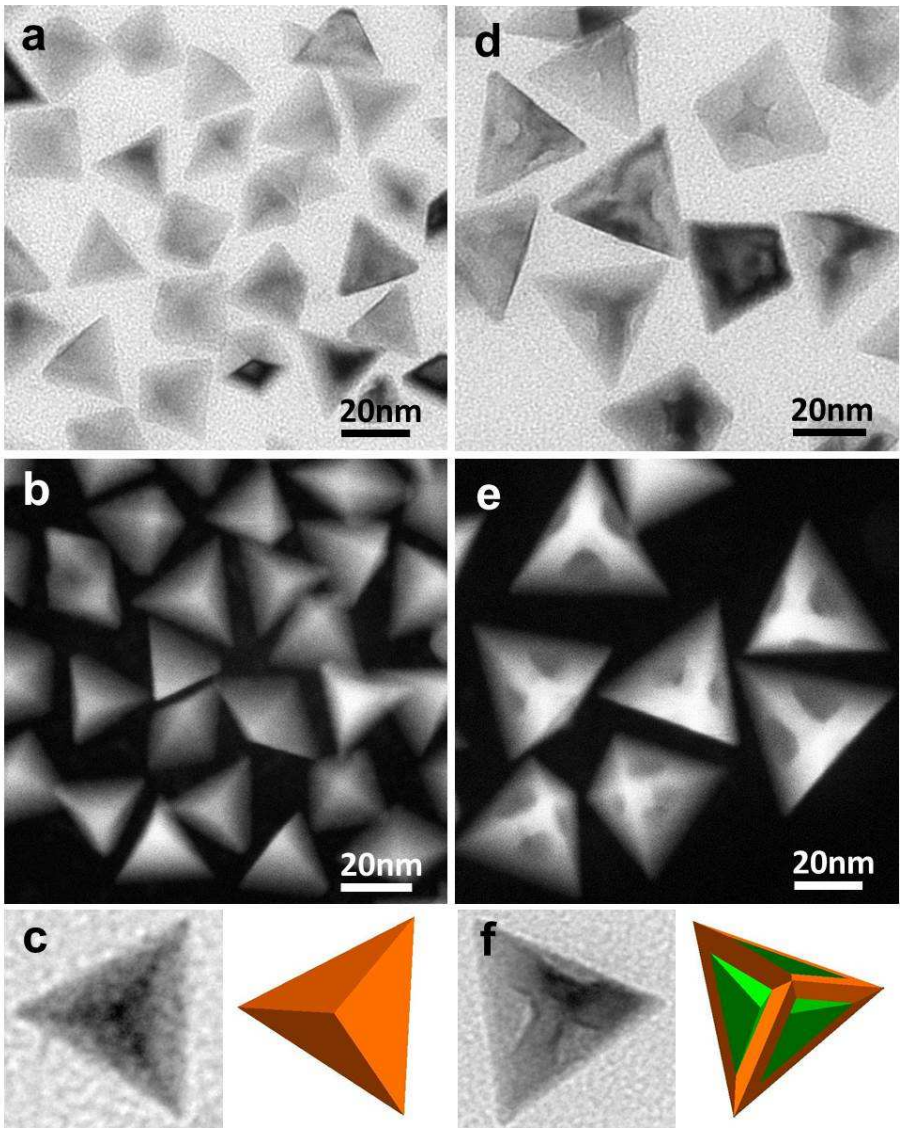

Figure 1. Representative TEM image (a) and HAADF-STEM image (b) of the Pd tetrahedra. (c) TEM image and corresponding geometric model of an individual Pd tetrahedron. Representative TEM image (d) and HAADF-STEM image (e) of the Pd concave tetrahedra. (f) TEM image and corresponding geometric model of an individual Pd concave tetrahedron.

Significantly, when we introduced a small amount of water with other growth parameters identical to the synthesis of Pd concave tetrahedra, unique Pd nanosheets were generated (**Figure 2 and Figure S3**). The representative TEM and HAADF-STEM images are shown in **Figure 2a-d and Figure S3**, which

clearly showed that the product consisted of sheet-like structures with a typical yield approaching 87%. The majority of the byproduct is Pd concave tetrahedra. The unique Pd nanosheets had an average edge length of 124 nm and a thickness of only about 2.3 nm (**Figure 1e**). Interestingly, each nanosheet was corolla-like with multibranched subunits. This striking feature is clearly apparent in the high-magnification TEM and HAADF-STEM images (**Figure 2b, 2d**). Both selected area electron diffraction (SAED) and HRTEM measurements (**Figure 2f, 2g**) on individual nanosheet indicated the single-crystalline nature of the corolla-like Pd nanosheet. The SAED pattern showed a series of diffraction spots with six-fold rotational symmetry. The HRTEM image showed lattice fringes with interplanar spacing of 0.24 nm, corresponding to 1/3(422) fringes of *fcc* Pd (**Figure 2g**). These results suggest that the obtained Pd nanosheet has basal (111) plane and stacking faults parallel to the basal (111) plane.[24,30] The *fcc* structure of the Pd nanosheets is also supported by their PXRD pattern (**Figure S1**).

The achievement of creating unique Pd nanosheets without the use of any toxic carbon monooxide or metal carbonyl is the most striking feature of the synthesis shown herein.[24,27] To gain better understanding of the growth mechanism for the synthesis of Pd nanosheets, Pd concave tetrahedra and also the Pd tetrahedra, we designed sets of experiments to investigate how the reaction kinetics and/or etching affect the proceeding of reactions and thus the final different shapes. The structure evolution process for Pd nanosheets, Pd concave tetrahedra and also the Pd tetrahedra were summarized in **Figure 3**, **Figure S4**, and **Figure S5**, respectively. Specifically, the products collected at 15 min were hexagonal Pd nanosheets with an average edge length of 49 nm. Noticeably, the nanosheets collected at 30 min were slightly etched at their edges. The average size of this nanosheet was 93 nm. The nanosheets increased to 122, 123, 122, and 124 nm in size when the reaction time was prolonged to 60, 120, 480, and 600 min, respectively. During the growth of the nanosheets, their etched feature also became more and more prominent. After 480 min, no further change in the size or the morphology of the

nanosheets was observed (**Figure 3**). Therefore, these results imply that the etched sites likely resulting from iron species oxidation at the early stage of the synthesis served as the growth sites for forming the corolla-like nanosheets.[35] For the Pd concave tetrahedra, small Pd concave tetrahedra were already formed at 15 min. The size of the Pd concave tetrahedra increased with prolonged reaction time. It was observed that the concave feature of the nanocrystals was maintained throughout the whole growth process. These results imply that the concave feature was developed at the very beginning and concomitant with the growth process (**Figure S4**). Similar growth process was found in the case of Pd tetrahedra, where small Pd tetrahedra were already formed at the early stage and the size of the Pd tetrahedra enlarged with increasing reaction time (**Figure S5**).

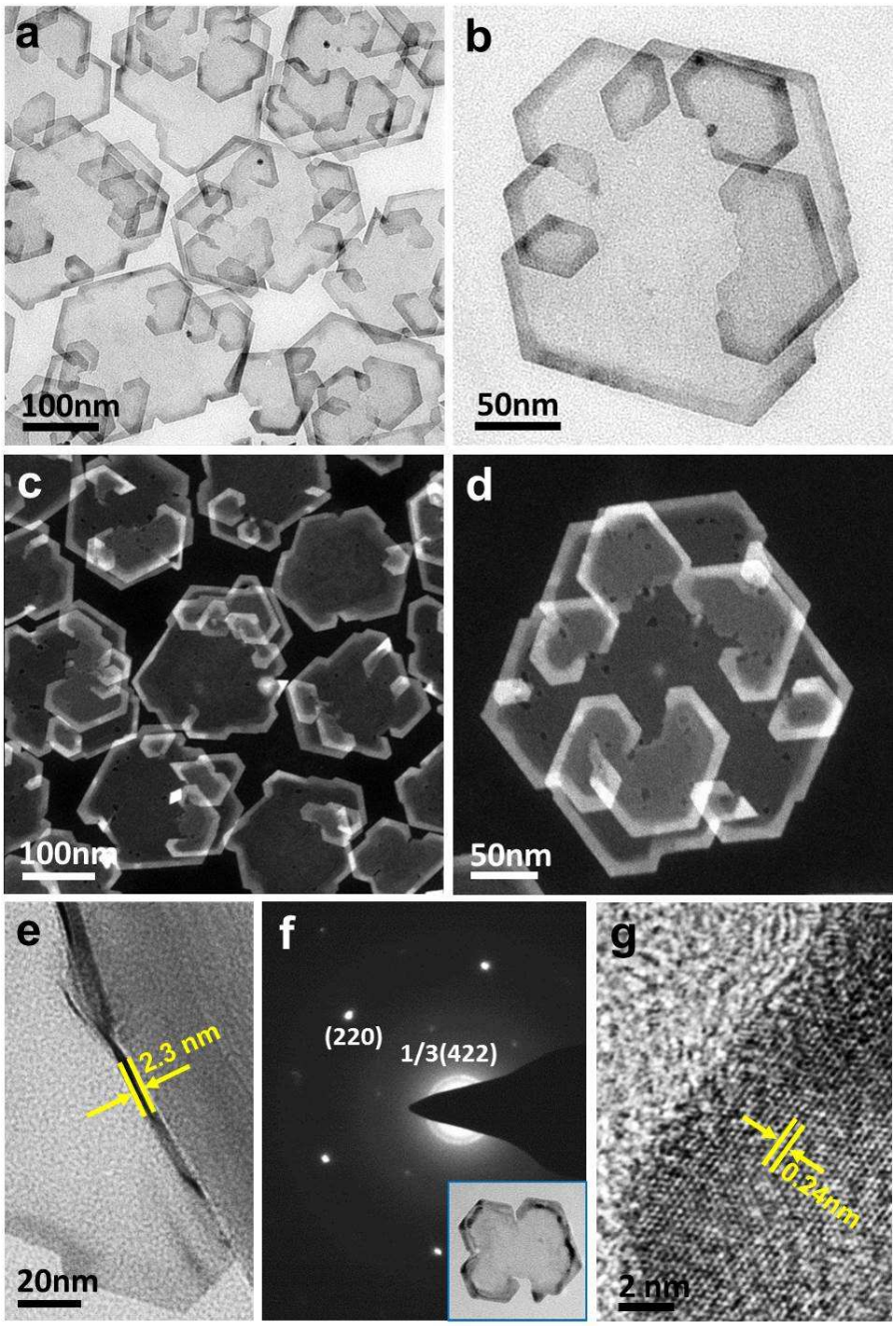

Figure 2. (a, b) TEM images and (c, d) HAADF-STEM images of the Pd nanosheets. (e) TEM image of a single Pd nanosheet attached on a carbon nanotube. (f) SAED pattern of a single Pd nanosheet. Bottom-right inset shows the corresponding TEM image. (g) HRTEM image on the edge of a Pd nanosheet.

The critical role of H_2O in the growth of the unique Pd nanosheets is quite unexpected. To try to understand the critical role of H_2O in controlling the synthesis of Pd nanosheets, we have conducted additional experiments to thoroughly investigate the impacts of different amount of H_2O on the synthesis of Pd nanosheets. As illustrated by TEM analyses, only Pd concave tetrahedra were obtained in the absence of any H_2O (**Figure S6**). The population of Pd tetrahedra decreases and the population of Pd nanosheets increases with increasing the amount of H_2O to 0.5% water in DMF. The Pd nanosheets with high yield were obtained at 1% water in DMF and onward (1.5% water in DMF) (**Figure S6**). Based on the controlled experiments, we infer that the specific and appropriate amount of H_2O is essential to grow the Pd nanosheets, possibly due to the optimal kinetic growth of Pd nanosheets corresponding to the specific H_2O concentration. In many previous wet chemical synthesis, the introduction of specific additives has been proved to be an effective strategy to control metal nanocrystals.[3] Further deeper understanding of such controlled synthesis are likely due to the ability to precise control of the reaction kinetics by introduction of additives.[26,30] In our present synthesis of Pd nanosheets, we visually observed that the addition of H_2O could retard the reduction, as the reaction mixture containing H_2O changed more slowly than that of reaction without H_2O. We therefore measured the formation of Pd nanocrystals at different synthesis time to qualitatively calculate the reduction kinetics responsible for the formation of Pd nanosheets, Pd concave tetrahedra, and Pd tetrahedra. The percent conversions of $Pd(acac)_2$ as a function of reaction time for the standard syntheses of Pd nanosheets, Pd concave tetrahedra, and Pd tetrahedra are shown in **Figure S7**. At t = 15 min, the conversions were 2.8%, 10.7% and 21.0% for the cases of Pd nanosheets, Pd concave tetrahedra and Pd tetrahedra, respectively. At t = 120 min, the corresponding conversions became 35.6%, 67.5% and 75.5%, respectively. On the basis of the above studies, it can be concluded that the reduction rate of the precursor is in the order of Pd tetrahedra > Pd concave tetrahedra > Pd nanosheets. Our results suggest that distinct Pd nanocrystals from Pd nanosheets to Pd tetrahedra have been obtained by simply introducing AA and/or water without all other parameters

changed. Because the type of additives can affect the reduction kinetics, the initial reduction rate of a synthesis is responsible for the formation of seeds with different structures. In our synthesis, while a fast reduction rate is responsible for the growth of single crystal Pd tetrahedra, a slow reduction rate is beneficial for the growth of Pd nanosheets with stacking faults, which is consistent with the recent published results, where Pd nanoplates were the major products when the reduction rate was reduced in the low synthesis temperature.[30] Therefore, by controlling the reduction rate of a synthesis, we could obtain Pd nanocrystals with distinctive structures.

To achieve better control of the growth of Pd nanosheets, we also thoroughly investigated the impacts of the other synthesis reagents on the growth of Pd nanosheets. As showed in **Figure S8**, the reaction in the absence of AA cannot produce Pd nanosheets. The formation of Pd nanosheets was observed once AA was introduced into the synthesis, even though the quality of the Pd nanosheets is dependent on the amount of AA added (**Figure S8**). As showed in **Figure S9**, when AA are replaced with citric acid, the product containing the mixture of polyhedra are obtained, indicating that the AA is also an important shape-directing agent in the growth of Pd nanosheets. To understand why nanosheets could not form when AA was replaced by citric acid, we further analyzed the intermediates collected at different stages when citric acid was used. We observed that the reaction mixture containing citric acid was unchanged and no separable particles were obtained from the reaction until 15 min. This phenomenon indicates that the citric acid greatly retarded the reduction of $Pd(acac)_2$. Pd nanocrystals collected at 30 min were irregular nanoparticles with different shapes. The average size of the nanocrystals increased when the reaction time was prolonged (**Figure S10**). Because the type of additives can affect the coordinating environment and thus the reduction kinetics, the initial reduction rate of a synthesis is responsible for the formation of seeds with different structures during the nucleation. Since citric acid is a very strong tridentate agent, it is reasonable to think that the citric acid

will heavily affect the nucleation and thus the formation of Pd nanosheets. In addition to the critical role of AA, the use of $Fe(acac)_2$ are also important for the growth of Pd nanosheets. As confirmed by the SEM-EDX, the presence of Fe species was also detected in the final product even after severe wash (**Figure S11**). It seems that high-quality of Pd nanosheets can only be prepared in a certain amount of $Fe(acac)_2$, as shown in **Figure S12**. In the synthesis of Pd nanosheets, we have also studied the effect of the Pd precursor concentrations on the synthesis of the Pd nanosheets. It turns out that the high concentration of the Pd precursors is not beneficial for the production of Pd nanosheets with high purity (**Figure S13**).

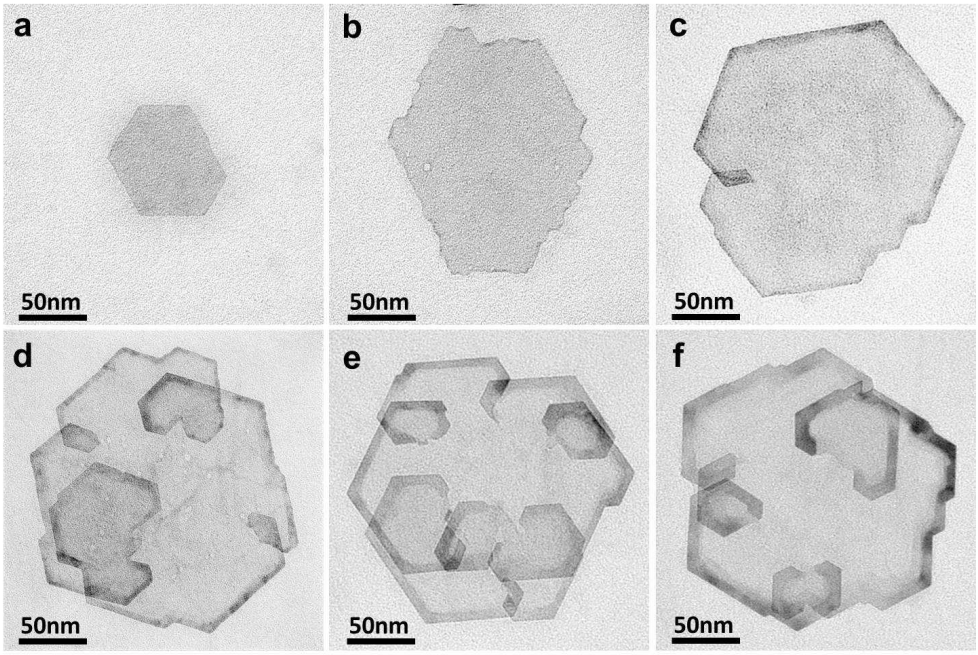

Figure 3. TEM images of Pd nanosheet intermediates produced in (a) 15, (b) 30, (c) 60, (d) 120, (e) 480, and (f) 600 min reactions.

Although great success has been achieved on the controlled preparation of Pd nanocrystals with different sizes and morphologies, a robust approach to systematic production of well-defined nanostructures without seeds remains a significant challenge. The realization of production of Pd

nanocrystals with highly controlled fashion is highly beneficial for studying shape-dependent properties. Nanostructured Pd nanocrystals are active catalyst for various organic reactions and have remarkable performance in electrooxidation of small organic molecules and hydrogenation reactions.[1,36] To this end, we first chose the formic acid electrooxidation as a model reaction to investigate the catalytic performance of as-made Pd nanocrystals. The commercial Pd black was chosen as reference for comparison (**Figure S14**). **Figure 4a** shows the cyclic voltammetry (CV) curves of Pd nanosheets, Pd concave tetrahedra, Pd tetrahedra and Pd black recorded at room temperature in 0.1M $HClO_4$ solution at a sweep rate of 50 mVs^{-1}. According to the CV curves shown in **Figure 4a**, the electrochemical surface areas (ECSAs) were calculated as 35.6 m^2g^{-1} for Pd nanosheets, 18.3 m^2g^{-1} for Pd concave tetrahedra, 16.7 m^2g^{-1} for Pd tetrahedra and 15.5 m^2g^{-1} for Pd black. **Figure 4b** shows the CV curves of those Pd nanomaterials recorded at room temperature in 0.1M $HClO_4$ + 0.2 M HCOOH solution at a sweep rate of 50 mVs^{-1}. The current density was normalized over the Pd loading to give the mass activity (**Figure 4b**). We find that the mass activities follow the order of Pd nanosheets > Pd concave tetrahedra > Pd tetrahedra > Pd black. The mass activity of Pd nanosheets is measured to be 634.3 $mAmg^{-1}_{Pd}$, which is 1.38 times, 2.67 times and 3.51 times higher than those of the Pd concave tetrahedra, Pd tetrahedra and Pd black, respectively (**Figure 4b**). Furthermore, the durability of all the Pd catalysts were tested by repeating the CV sweeps for 200 cycles (**Figure 4c**). After 200 sweeping cycles, 54% of the initial catalytic activity was still maintained for the Pd nanosheets (28.3% for Pd concave tetrahedra and 33.7% for Pd tetrahedra), as compared with the loss of 96% for Pd black, highlighting a better catalytic stability of the as-made Pd nanocrystals.

To investigate the catalytic differences of the prepared Pd nanocrystals as hydrogenation catalysts, the hydrogenation of styrene was selected and carried out at room temperature. In a typical hydrogenation of styrene, styrene was readily converted into ethylbenzene over different Pd nanocrystals

by using hydrogen gas as the hydrogen source and ethanol as the solvent. **Figure 4d** shows the plots of conversion of styrene against time after the addition of the Pd catalysts with the same amount of Pd. All the catalysts are effective catalysts for this hydrogenation reaction. However, the conversion efficiencies are different from each other. At t = 30 min, the conversions of styrene were 88%, 82%, 63%, and 38% for the Pd nanosheets, the Pd concave tetrahedra, the Pd tetrahedra, and the Pd black, respectively. Again, the activity of the Pd nanosheets is better than that of Pd concave tetrahedra, Pd tetrahedra, Pd black and the reason behind this could be attributed to the simple yet important ultrathin feature and thus high surface area of the Pd nanosheets.

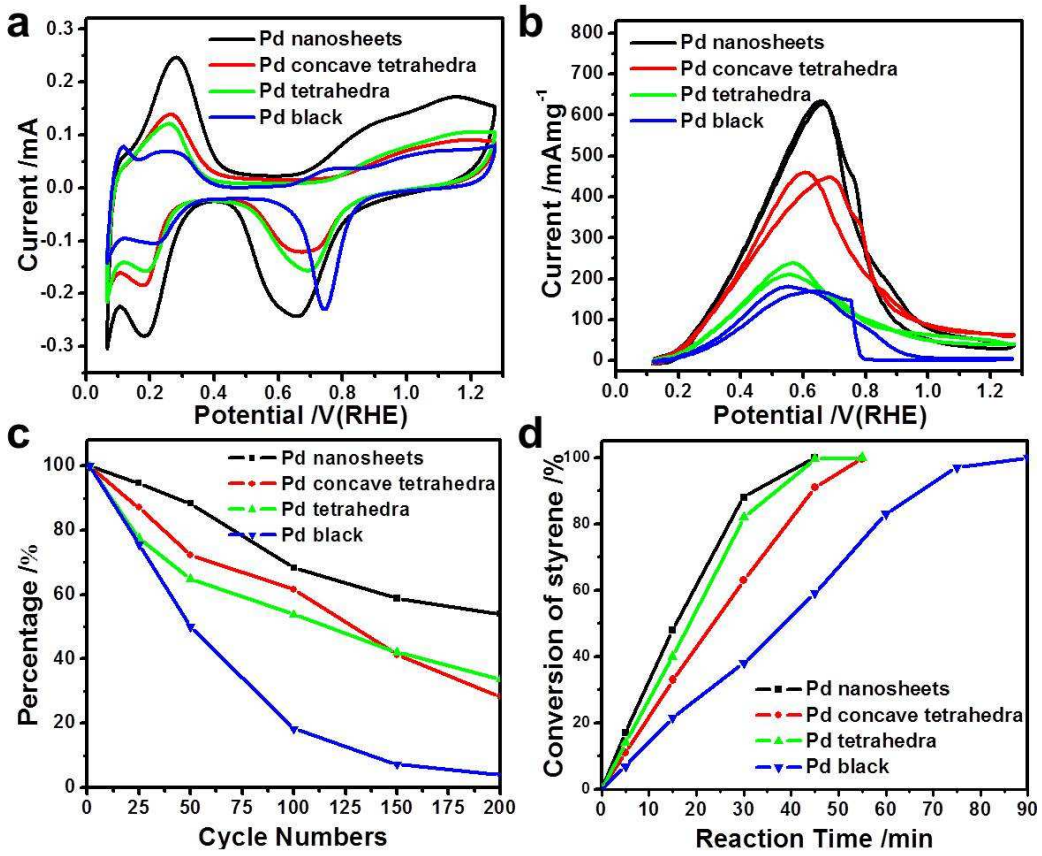

Figure 4. (a) Cyclic voltammograms and (b) formic acid oxidation curves recorded at room temperature of different Pd catalysts. (c) Variation of normalized peak current densities of electrooxidation in the positive-going potential sweep

during potential cycling. Potential was continuously scanned at 50 mVs^{-1} in 0.1 M $HClO_4$ + 0.2 M formic acid. (d) Conversion of styrene during hydrogenation reactions catalyzed by different Pd catalysts

To summarize, we have presented an efficient approach that can realize the production of well-defined Pd nanocrystals in a highly controllable fashion. Pd nanosheets, Pd concave tetrahedra and Pd tetrahedra have been selectively obtained with high yield. To the best of our knowledge, it is the first example that unique Pd nanosheets have been obtained without the use of any toxic and/or explosive carbon monooxide or metal carbonyls. These well-defined Pd nanocrystals herein represent an ideal platform for investigating the shape dependent properties and we have demonstrated that their properties are highly dependent on their morphologies. It has been showed that the unique Pd nanosheets can serve as highly efficient catalysts for both styrene hydrogenation and formic acid electrooxidation, where they outperformed the other two Pd polyhedra and commercial Pd black. These enhanced properties of Pd nanosheets can be attributed to their ultrathin feature that provides increased active sites. We expect these newly generated Pd nanocrystals with unique and tunable structure will enable various applications, such as fuel cell reactions, advanced catalysis and beyond.

ASSOCIATED CONTENT

Supporting Information. Experimental details and data. Figure S1-14. This material is available free of charge *via* the Internet at http://pubs.acs.org.

Corresponding Author

hxq006@suda.edu.cn; yhuang@seas.ucla.edu.

ACKNOWLEDGMENT

This work was financially supported by the start-up funding from Soochow University, Young Thousand Talented Program, Ralph E. Powe Junior Faculty Enhancement Award. E.Z and Y.H acknowledge support from the National Science Foundation (NSF) through award DMR-1437263.

The authors declare no competing financial interest.

References

1. Bianchini, C.; Shen, P. K. *Chem. Rev.* **2009**, 109, 4183.

2. Zhang, H.; Jin, M. S.; Xiong, Y. J.; Lim, B.; Xia, Y. N. *Acc. Chem. Res.* **2013**, 46, 1783.

3. Chen, M.; Wu, B.; Yang, J.; Zheng, N. *Adv. Mater.* **2012**, 24, 862.

4. Favier, F.; Walter, E. C.; Zach, M. P.; Benter, T.; Penner, R. M. *Science* **2001**, 293, 2227.

5. Nishihata, Y.; Mizuki, J.; Akao, T.; Tanaka, H.; Uenishi, M.; Kimura, M.; Okamoto, T.; Hamada, N. *Nature* **2002**, 418, 164.

6. Kim, S. W.; Kim, M.; Lee, W. Y.; Hyeon, T. *J. Am. Chem. Soc.* **2002,** 124, 7642.

7. Jin, M. S.; Zhang, H.; Xie, Z. X.; Xia, Y. N. *Angew. Chem. Int. Ed*. **2011**, 50, 7850.

8. Crespo-Quesada, M.; Yarulin, A.; Jin, M.; Xia, Y.; Kiwi-Minsker, L. *J. Am. Chem. Soc.* **2011**, 133, 12787.

9. Li, G.; Kobayashi, H.; Dekura, S.; Ikeda, R.; Kubota, Y.; Kato, K.; Takata, M.; Yamamoto, T.; Matsumura, S.; Kitagawa, H. *J. Am. Chem. Soc.* **2014**, 136, 10222.

10. Li, G.; Kobayashi, H.; Taylor, J. M.; Ikeda, R.; Kubota, Y.; Kato, K.; Takata, M.; Yamamoto, T.; Toh, S.; Matsumura, S.; Kitagawa, H. *Nat. Mater.* **2014**, 13, 802.

11. Xia, Y. N.; Xiong, Y. J.; Lim, B.; Skrabalak, S. E. *Angew. Chem. Int. Ed.* **2008**, 48, 60.

12. Oliver-Meseguer, J.; Cabrero-Antonino, J. R.; Dominguez, I.; Leyva-Perez, A.; Corma, A. *Science* **2012**, 338, 1452.

13. Turner, M.; Golovko, V. B.; Vaughan, O. P. H.; Abdulkin, P.; Berenguer-Murcia, A.; Tikhov, M. S.; Johnson, B. F. G.; Lambert, R. M. *Nature* **2008**, 454, 981.

14. Wang, Z. L. *J. Phys. Chem. B* **2000**, 104, 1153.

15. Tian, N.; Zhou, Z. Y.; Sun, S. G. *J. Phys. Chem. C* **2008**, 112, 19801.

16. Xiong, Y.; McLellan, J. M.; Chen, J.; Yin, Y.; Li, Z.; Xia, Y. *J. Am. Chem. Soc.* **2005**, 127, 17118.

17. Lim, B.; Xiong, Y.; Xia, Y. *Angew. Chem., Int. Ed.* **2007,** 46, 9279.

18. Tian, N.; Zhou, Z.; Yu, N.; Wang, L.; Sun, S. *J. Am. Chem. Soc.* **2010**, 132, 7580.

19. Xia, X.; Choi, S.; Herron, J. A.; Lu, N.; Scaranto, J.; Peng, H.; Wang, J.; Mavrikakis, M.; Kim, M. J.; Xia, Y. *J. Am. Chem. Soc.* **2013**, 135, 15706.

20. Li, C.; Sato, R.; Kanehara, M.; Zeng, H.; Bando, Y.; Teranishi, T. *Angew. Chem., Int. Ed.* **2009**, 48, 6883.

21. Huang, X.; Zheng, N. *J. Am. Chem. Soc.* **2009**, 131, 4602.

22. Huang, X.; Tang, S.; Zhang, H.; Zhou, Z.; Zheng, N. *J. Am. Chem. Soc.* **2009**, 131, 13916.

23. Dai, Y.; Mu, X.; Tan, Y.; Lin, K.; Yang, Z.; Zheng, N.; Fu, G. *J. Am. Chem. Soc.* **2012**, 134, 7073.

24. Huang, X.; Tang, S.; Mu, X.; Dai, Y.; Chen, G.; Zhou, Z.; Ruan, F.; Yang, Z.; Zheng, N. *Nat. Nanotechnol.* **2011**, 6, 28.

25. Huang, X.; Li, Y.; Chen, Y.; Zhou, E.; Xu, Y.; Zhou, H.; Duan, X.; Huang, Y. *Angew. Chem. Int. Ed.* **2013**, 52, 2520.

26. Huang, H.; Wang, Y.; Ruditskiy, A.; Peng, H. C.; Zhao, X.; Zhang, L.; Liu, J.; Ye, Z.; Xia, Y. *ACS Nano* **2014**, 8, 7041.

27. Yin, X.; Liu, X.; Pan, Y; Walsh, K. A.; Yang, H. *Nano Lett.* **2014**, 14, 7188.

28. Wang, F.; Li, C.; Sun, L.; Xu, C.; Wang, J.; Yu, J. C. Yan, C. *Angew. Chem., Int. Ed.* **2012**, 51, 4872.

29. Niu, Z.; Peng, Q.; Gong, M.; Rong, H.; Li, Y. *Angew. Chem., Int. Ed.* **2011**, 50, 6315.

30. Wang, Y.; Peng, H.; Liu, J.; Huang, C. Z.; Xia, Y. *Nano Lett.* **2015**, 15, 1445.

31. Zhu, C.; Zeng, J.; Lu, P.; Liu, J.; Gu, Z.; Xia, Y. *Chem. Eur. J.* **2013**, 19, 5127.

32. Wang, Y.; Xie, S.; Liu, J.; Park, J.; Huang, C. Z.; Xia, Y. *Nano Lett.* **2013**, 13, 2276.

33. Niu, W.; Zhang, L.; Xu, G. *ACS Nano* **2010**, 4, 1987.

34. Chen, Y. H.; Hung, H. H.; Huang, M. H. *J. Am. Chem. Soc.* **2009**, 131, 9114.

35. Huang, X.; Tang, S.; Yang, J.; Tan, Y.; Zheng, N. F. *J. Am. Chem. Soc.* **2011**, 133, 15946.

36. Somorjai, G. A.; Li, Y. M. *Top. Catal.* **2010,** 53, 832.